Energy Conversion and Management: X 30 (2026) 101845

Contents lists available at ScienceDirect

Energy Conversion and Management: X

journal homepage: www.sciencedirect.com/journal/energy-conversion-and-management-x

Proof of concept of a latent heat thermal energy storage system based on the Rotating Drum Heat Exchanger for on-demand steam supply

Jonas Tombrink *, Andrea Gutierrez

German Aerospace Center (DLR), Institute of Engineering Thermodynamics, Pfaffenwaldring 38-40, 70569 Stuttgart, Germany

ARTICLE INFO

Keywords:
Rotating Drum Heat Exchanger
Latent heat thermal energy storage
Experimental demonstration
Phase change material
Renewable process steam
Power-to-heat

ABSTRACT

To provide a cost-effective and CO_2-free solution for the on-demand provision of process steam for industrial application, the storage of thermal energy from fluctuating renewable energy sources enables the efficient decoupling of energy supply and demand. In this study, a latent heat thermal energy storage system for the provision of process steam was designed, built and experimentally demonstrated. A custom-designed Rotating Drum Heat Exchanger, which is the key component for steam generation during discharge of the storage system, was experimentally investigated. At this heat exchanger a Phase Change Material (PCM) solidifies on the outer surface of the rotating drum, which is partially immersed into liquid PCM, while the released phase change enthalpy is transferred to water that it is fed through the inner wall of the drum, evaporating and exiting the drum as saturated steam. The technology is experimentally investigated using a drum with a total outer surface area of 1.1 m^2 and 400 kg of the eutectic mixture of sodium nitrate and potassium nitrate, with a melting point of 222 °C as PCM. The setup described in detail in this study, successfully demonstrates process steam generation at a pressure of up to 8 bar abs and a thermal power of up to 70 kW. The experimental methodology is validated, providing a foundation for a further comprehensive characterization and development of this technology.

Introduction

Thermal energy accounts for almost half of world's total final energy demand [1]. In Europe, the industrial demand for thermal energy in the temperature range between 100 °C and 400 °C amounts to 5% of the total final energy demand corresponding to around 600 TWh per year [2,3]. Process steam is an important energy carrier in this temperature range, which is currently mainly provided by steam boilers using fossil fuels [4].

The electrification of the heat sector is one of the key strategies of the EU to reduce CO_2-emissions, as electrical energy can be generated cost-effectively from renewable energy sources such as wind and solar [5]. However, additional effort is required in terms of energy storage to overcome the fluctuating nature of these energy sources. While electrochemical energy storage is available and allows charging and discharging of energy in form of electricity, storing the energy directly in the required form of thermal energy may offer cost advantages and reduces the need of critical materials [6].

In the temperature range between 100 °C and 200 °C, typical for processes such as drying, distilling, cooking and space heating, High Temperature Heat Pumps (HTHP) are gaining attention as promising solution for a carbon-neutral thermal energy supply. While HTHP have the advantage of a Coefficient of Performance (COP) larger than one, meaning they can provide more than one-unit of thermal energy while requiring one unit of electricity, there are technical limitations for their use. Firstly, the sink temperature is limited to <160 °C [4,7]. A further limitation in the implementation of highly efficient HTHP is the need for the availability of a suitable heat source in the form of waste heat, which must be available in synchronization with the demand for high-temperature thermal energy. For a thermodynamic efficient conversion of low temperature to high temperature heat, the difference between the heat source and the heat sink should be below 100 K [8,9]. For an increased sink temperature of HTHPs, steam is also a promising working fluid. Furthermore, low temperature and low-pressure steam might be compressed back to higher pressures and reused directly, a process known as mechanical vapor recompression (MVR). There are intensive research activities to develop these components for higher temperatures, however high temperatures also hinder the implementation of these components because, in addition, suitable lubricants and sealants have to be developed [9,10].

A direct electrical heat supply via resistive heating limits the

* Corresponding author.
E-mail address: jonas.tombrink@dlr.de (J. Tombrink).

https://doi.org/10.1016/j.ecmx.2026.101845
Received 14 November 2025; Received in revised form 16 March 2026; Accepted 9 April 2026
Available online 13 April 2026
2590-1745/© 2026 The Author(s). Published by Elsevier Ltd. This is an open access article under the CC BY license (http://creativecommons.org/licenses/by/4.0/).

Nomenclature

Latin

c	heat capacity, $[c] = \mathrm{J{\bullet}kg^{-1}{\bullet}K^{-1}}$
c_p	heat capacity at constant pressure, $[c_p] = \mathrm{J{\bullet}kg^{-1}{\bullet}K^{-1}}$
D	(Drum)Diameter, $[D] = \mathrm{m}$
h	specific enthalpy, $[h] = \mathrm{J{\bullet}kg^{-1}}$
k	thermal conductivity, $[k] = \mathrm{W{\bullet}m^{-1}{\bullet}K^{-1}}$
L	Length $[L] = \mathrm{m}$, Phase Changer Enthalpy, $[L] = \mathrm{J{\bullet}kg^{-1}}$
$\dot{m}$	mass flow, $[\dot{m}] = \mathrm{kg{\bullet}s^{-1}}$
n	Rotational Speed, $[n] = \mathrm{s^{-1}}$
P	Power, $[P] = \mathrm{W}$
p	pressure, $[p] = \mathrm{bar}$
$\dot{Q}$	heat flux, $[\dot{Q}] = \mathrm{W}$
$\dot{q}$	surface-specific heat flux, $[\dot{q}] = \mathrm{W{\bullet}m^{-2}}$
s	(wall) thickness, $[s] = \mathrm{m}$
T	Temperature, $[T] = {}^{\circ}\mathrm{C}$

Greek

σ	yield strength, $[\sigma] = \mathrm{N{\bullet}m^{-1}}$, Surface Tension, $[\sigma] = \mathrm{N{\bullet}m^{-1}}$
η	dynamic viscosity, $[\eta] = \mathrm{Pa{\bullet}s}$
ϱ	Density, $[\varrho] = \mathrm{kg{\bullet}m^{-3}}$
ϕ	Immersion angle, $[\phi] = {}^{\circ}$ Deg

Mathematical Symbols

d	differential
$\int$	integral

Sub-/Superscripts

$\bar{}$	averaged
$'$	saturated liquid
$''$	saturated gas
l	liquid
m	melting
PCM	Phase Change Material
RD	Rotating Drum
s	solid, isentropic
sat	saturated (Water, Steam)
Δh	Enthalpy difference method
ΔT	Temperature difference method

Abbreviations

HTHP	High Temperature Heat Pump
COP	Coefficient of Performance
PCM	Phase Change Material
HTF	Heat Transfer Fluid
LHTES	Latent Heat Thermal Energy Storage
$NaNO_3$	Sodium Nitrate
KNO_3	Potassium Nitrate
(eu)	eutectic Mixture

theoretical COP to values below one; nevertheless, they can be used without restrictions of a required heat source, as in the case of HTHP. In addition, the maximum operating temperature range is limited by the material properties of the resistive heaters and the heated materials. Therefore, the specific heat transfer can be increased by increasing the maximum temperature of the heater, without reducing the COP and keeping it close to one. This as well as the simplicity of resistive heating decreases the investment costs of these heaters.

Decoupling the demand for thermal energy from the availability of renewable electrical energy not only enables a higher degree of direct use of any self-generated renewable energy that may be available, but can also enable a reduction in the purchase price of electricity. Fig. 1 illustrates how the wholesale electricity price varies throughout the day, with the values shown as averages for each hour and differentiated by season for Germany, Spain and California in 2023. Depending on the season, savings of up to 20% can be made on electricity costs if it is purchased only during the off-peak periods, what typically occurs at night and around midday. Further savings are possible with an optimized purchase strategy.

The most common commercial solution for large-scale thermal energy storage systems is the two-tank molten salt storage, which has been demonstrated at the GWh scale and was originally developed for Concentrated Solar Power (CSP) plants. Alternatively, instead of thermal charging, these storages can also be charged electrically, e.g., by using resistive heaters, as proposed and calculated economically for industrial heat supply in [11]. A widely used storage material of two-tank molten salt storage is so-called solar-salt, a mixture of 40 wt% potassium nitrate and 60 wt% sodium nitrate, typically used in the temperature range between 290 °C and 560 °C, resulting in a storage capacity of 200 kWh/m^3 [12]. Thereby, the total costs of the hot storage tank made of 321 stainless steel exceeds the costs of the cold storage tank made out of carbon steel by a factor of 2.2, while both storage tanks accounting for 38% of the cost of the storage system. The storage material accounts to 46% of the costs of the storage system [13].

This figures mainly show two options for reducing the specific investment costs of these thermal energy storage systems: On the one hand

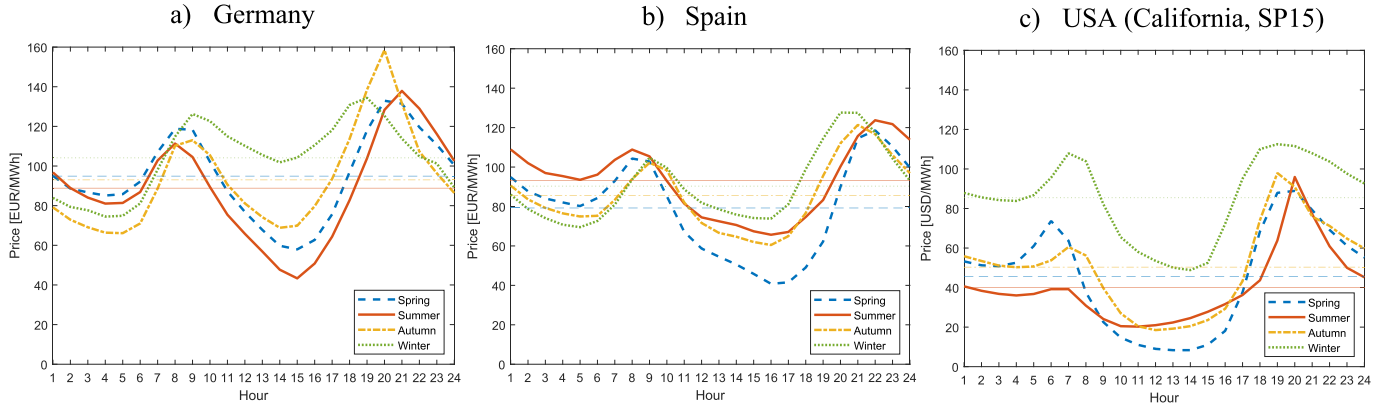

Fig. 1. Fluctuation of the electricity price in a) Germany, b) Spain, c) USA (California SP15) in 2023; mean value of the specific hour within the mentioned season. Spring: March-May; Summer June-August; Autumn: September-November; Winter: December-February [39,40].

by increasing the specific storage density of the storage material. This can be achieved, for example, by increasing the maximum operating temperature of the storage material, as proposed e.g. by Bonk et al. [14] who reports that the specific storage density can be increased by 16% by increasing the operating temperature in the hot tank up to 600 °C. On the other hand, the investment costs can be decreased by reducing the maximum operating temperature, which allows the use of more cost-efficient construction materials for both, the hot and the cold storage tanks. However, this option reduces the specific storage density. In both cases only sensible thermal energy is stored in the solar salt, and the material must be kept in the liquid phase during the whole operation to maintain its pumpability.

By extending the operating temperature rage to temperatures below the melting point or melting range of the storage material, the phase change enthalpy, i.e. the latent heat, can be utilized in addition to the sensible heat of the storage medium. This allows the specific energy storage density of the material to be increased without exceeding the upper temperature of 390 °C applicable to carbon steels. Considering the use of the eutectic mixture of sodium nitrate and potassium nitrate as storage medium (45.67 wt% $NaNO_3$; 54.33 wt% KNO_3), 206 kWh/m^3 can be stored if the system is operated in the temperature range between 170 °C and 390 °C [15]. In the case of using pure sodium nitrate as storage material, the specific storage density could be increased even to 215 kWh/m^3 in the same temperature range [16,17]. In both cases, the specific energy storage density is comparable to that reached by the state-of-the-art CSP hot tanks, however, the upper temperature in this case is limit to 390 °C, which allows the use of conventional carbon steel for both storage tanks. Further cost reductions can be expected for auxiliary components such as piping, valves, and pumps. Carbon steel shows good compatibility with nitrate salts under these temperature conditions [18,19].

If the maximum temperature is increased to the state-of-the-art limit of 560 °C, for which stainless steel is required for the hot storage tank, this results in storage capacities of 328 kWh/m^3 for the eutectic mixture of sodium nitrate and potassium nitrate and 353 kWh/m^3 for pure sodium nitrate. The storage densities are calculated according to the method mentioned in [20].

A technical solution to utilize the sensible heat as well as the latent heat by shifting the operating temperature of nitrate salts into a temperature range including the phase change between 170 °C and 390 °C is an active Latent Heat Thermal Energy Storages (LHTES) based on the so-called Rotating Drum Heat Exchanger.

This concept is visualised in Fig. 2. A drum is partially immersed into a tub of liquid Phase Change Material (PCM). While the PCM solidifies at the outer side of the rotating drum, a fluid flows through an annular gap inside the drum and changes phase from the liquid to the gaseous state. The phase change enthalpy, which is released by the phase change of the PCM from the liquid to the solid state, is transferred directly to the Heat Transfer Fluid (HTF), which undergoes a phase change from the liquid to the gaseous state. Since the PCM has a low thermal conductivity, the growing layer of solid PCM on the outer drum shell would limit the heat transfer. Therefore, this layer is transported by the rotation of the drum to a stationary scraper where the PCM is removed from the drums surface. A bare heat transfer surface is thus re-immersed into the liquid PCM, maximising the surface–specific heat transfer of the heat exchanger. By separating the solidified PCM from the drum shell after it has left the tub of liquid PCM, the solid PCM can be stored separately from the liquid PCM. This results in a total separation of the power and the capacity of a storage system based on the Rotating Drum Heat Exchanger, resulting in a high degree of design freedom. The concept was first published and experimentally validated with a liquid-only HTF and a low-temperature PCM in [21], providing a detailed investigation of the local heat transfer mechanisms and measurements of the resulting layer thicknesses. A numerical simulation approach has been published in [22] followed by a case study for a high-temperature system for process steam generation published in [20]. The latter publication also addresses the advantages and limitations of the Rotating Drum Heat Exchanger, especially regarding scalability and deployment in multi-MW applications.

The Rotating Drum Heat Exchanger for PCM investigated in this paper can be categorised as an active LHTES as the PCM is actively moved through the heat transfer surface in order to increase the heat transfer [23,24]. On the other hand, there are the so called passive LHTES were the PCM remains stationary. In passive concepts, the heat transfer from the solidification or melting of the PCM to the heat transfer surface and vice versa is usually increased by either increasing the thermal conductivity of the PCM itself or by introducing a heat transfer structure, e.g. in the form of fins made out of a material with high thermal conductivity [25,26]. In the present work, no additional heat transfer enhancing structures are used. While such structures could in principle also be implemented in an active concept, the investigated design intentionally relies on the continuous renewal of PCM at the heat

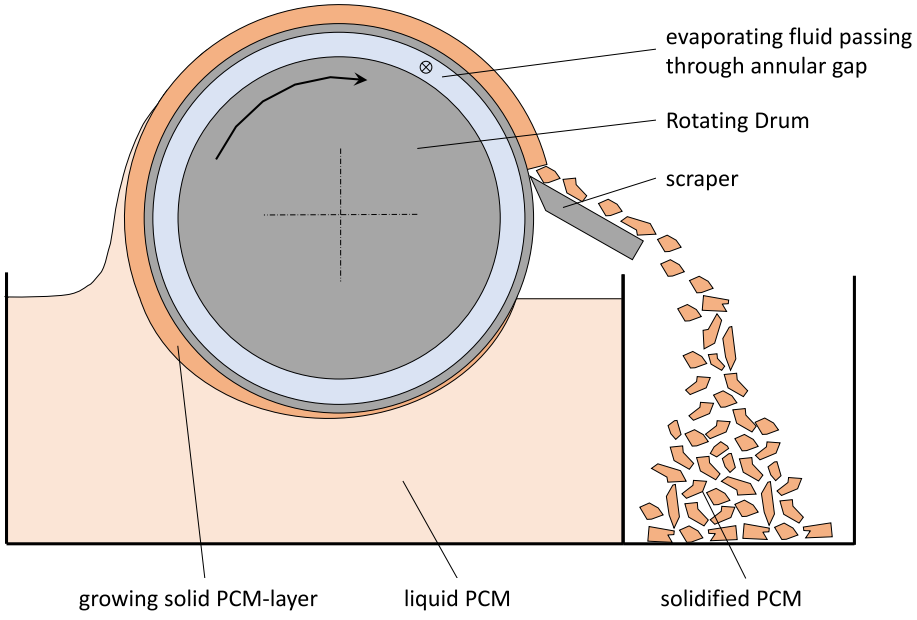

Fig. 2. Concept of the Rotating Drum Heat Exchanger for Phase Change Materials.

transfer surface through mechanical motion. This approach aims to maintain a high effective heat transfer rate and to enable comparatively high and stable thermal power levels as long as molten PCM is available. Furthermore, the absence of internal heat transfer structures simplifies the system design and operation.

Passive LHTES systems are technologically mature and have been demonstrated at multi-MWh scale, including in industrial applications [27]. As no moving components are required, they offer cost-effective and straightforward integration. However, the power-to-capacity ratio is inherently fixed by the design of the employed heat transfer structure, which can lead to disadvantages—particularly in applications requiring high capacity-to-power ratios.

Several concepts of active LHTES have been investigated through both simulation and experimental studies. Comprehensive reviews of the technology are available, for example in [23,24]. However, to the best of the author's knowledge, no active system has yet been demonstrated in multi-kW and/or multi-kWh range for the generation of steam.

In this paper, for the first time, an experimental proof-of-concept of an active LHTES for steam generation at the multi-kW scale and the usage of nitrate salt mixture as storage medium is provided, thereby providing a foundation for further development of this technology. This work continues the author's work previously published in [20–22]. This paper focuses on the thermal discharge process, meaning the generation of steam from solidifying nitrate salts. For recent scientific evaluations and improvements of efficient charging processes, particularly with regard to melting the PCM, reference is made to recent studies on close-contact melting, e.g. [28,29].

Description of the laboratory demonstrator

The demonstrator mainly consists of two separate circuits: The PCM-circuit and the water/steam-circuit. Both fluids meet at the Rotating Drum Heat Exchanger, where the PCM undergoes a phase change from its liquid to the solid state, while the water evaporates inside the rotating drum, which meaning that the latent heat of both fluids is transferred. Fig. 3 shows a simplified P&ID of the demonstrator. A detailed P&ID can be found in Appendix A. Pictures of the experimental setup can be seen in Fig. 4.

Water/steam circuit

Demineralised water is stored in an open feed water tank (CM101). A gear pump (GP101) with adjustable rotational speed to adjust the mass flow is used to increase the pressure of the water and to pump the water to the Rotating Drum Heat Exchanger (EP101). Here the water evaporates and steam leaves the drum. The pressure in the drum is regulated by an adjustable expansion valve (QN102) at the outlet of the drum. To close the circuit and to simulate steam demand, a condenser (EP102) is located downstream of the expansion valve and the condensate is given back into the feed water tank (CM101). A water reservoir (CM301) with a capacity of 800 l is used to cool the condenser via a pump (GP301), as the available cooling water supply of the used laboratory is insufficient.

The mass flow rate of the feed water is measured with a Coriolis

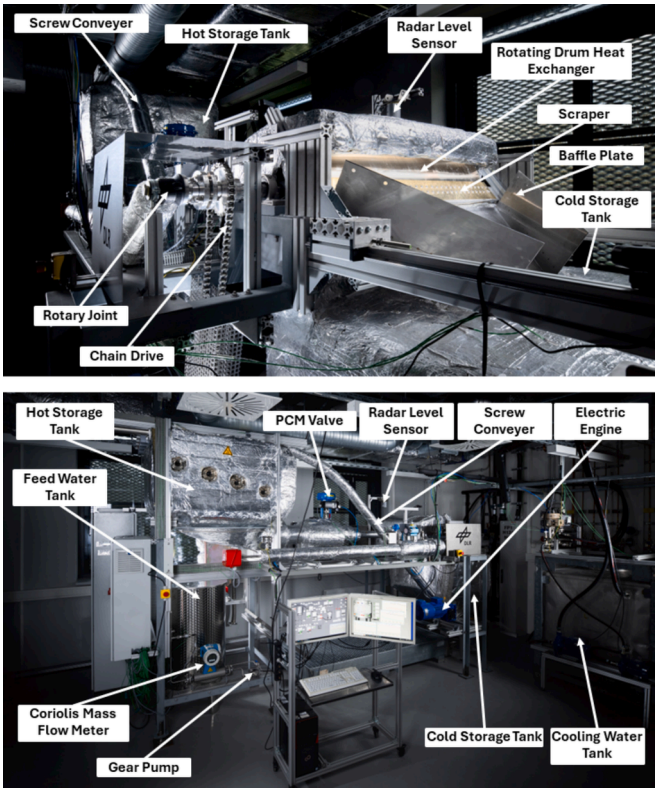

Fig. 4. Picture of the experimental test rig.

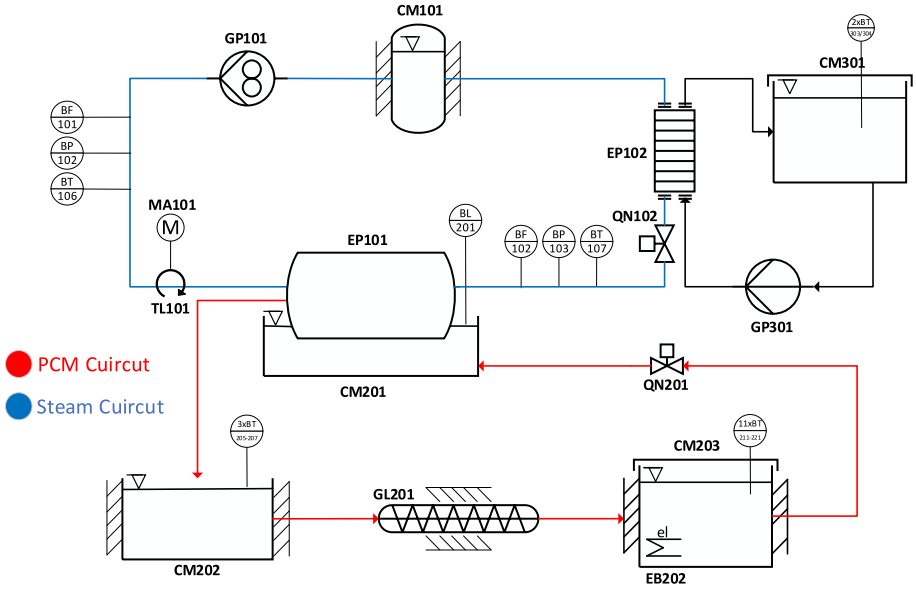

Fig. 3. Simplified P&ID of the experimental test rig.

measuring device (BF101) at the outlet of the gear pump. In addition, a vortex flow meter (BF102) is used at the outlet of the drum to measure the volume flow of the steam produced. By using a vortex flow meter, only the volumetric flow of the steam is measured due to the nature of the measuring principle. PT 100 temperature probes are used at the inlet of the drum (BT106) and at the outlet of the drum (BT107). The measurement of the water/steam circuit is supplemented by pressure sensors at the pump outlet (BP101), at the drum inlet (BP102) and at the drum outlet (BP103). The temperature of the water in the reservoir (CM301) is measured with two thermocouples (BT303 and BT304).

The detailed P&ID in appendix A also shows an electric heater (EB102) for regulating the temperature of the water at the inlet to the Rotating Drum Heat Exchanger. This was integrated into the test rig but not used during the experiments. A condensate drain (QN101) is installed to prevent droplet erosion in the steam pipe. A check valve (RM101), a ball valve (QM101) and a pressure relief valve (FL101) are integrated for safety reasons. Expansion joints (RR101 and RR102), rotary unions (UP101 and UP102) and pillow blocks (UP103 and UP104) are used to connect the Rotating Drum Heat Exchanger to the water/steam circuit.

Thermal insulation has been applied to the experimental test rig, taking into account the requirements for accessibility and visual observation during operation. The steam/water circuit is sufficiently insulated from the temperature and pressure measurement points BT106 and BP102 at the inlet of the rotating drum to the measurement points BT107 and BP103 at the outlet of the rotating drum. Nevertheless, large portions of the rotating drum remain openly accessible to allow the attachment and operation of the scraper, as shown in Fig. 4.

PCM circuit

To store the PCM, a cold storage tank (CM202) for the solid particles of the PCM and a hot storage tank (CM203) for storing the PCM in its liquid state are used. The PCM is transported from the cold storage tank to the hot storage tank using a screw conveyer (GL201). Electrical heaters (EB202) located in the hot storage tank are used to melt and temper the PCM. As the hot storage tank is at the highest level, there is a gradient in the pipe to guide the liquid PCM into the tub (CM201) below the Rotating Drum Heat Exchanger. The mass flow of the liquid PCM is adjusted by a pneumatic control valve (QN201) according to the level in the tub below the rotating drum, which is measured by a radar sensor (BL201). After the PCM has been removed from the outer surface of the rotating drum, the PCM flakes fall down into the cold tank (CM202). The mass flow of the PCM is not measured. Suitable high temperature flow meters are technically available, but the cost is high and the scientific benefit for the evaluation of the Rotating Drum Heat Exchanger is limited. To ensure a constant test environment, the level of liquid PCM in the tub below the drum (CM201) is kept constant by adjusting the regulation valve (QN201).

In the detailed P&ID in Appendix A, a trace heating (EB203) is shown on the liquid PCM pipe, which is used to prevent solidification in the pipe. A compensator (RR201) reduces the thermomechanical stress and a manually operated shut-off valve (QM201) is used as a backup valve. The electric heater (EB201) in the tub (CM201) below the rotating drum is mainly used during the start-up of the test rig to melt the PCM in this tub, but also to ensure a constant temperature of the liquid PCM during the experiments.

Thermal insulation has been applied to the PCM circuit primarily to ensure safe and controllable operation of the test rig and to limit heat losses to the environment. Since the electrical energy used for melting the PCM is not measured and the PCM circuit is therefore not independently quantified, the applied thermal insulation mainly serves to maintain stable and steady-state thermal conditions of the PCM.

The Rotating Drum Heat Exchanger

The key component of the storage system is the so-called Rotating Drum Heat Exchanger. In the system demonstrated, a drum with a length L of 1 m and an outer diameter D of 0.355 m is used. To ensure a constant flow of water through the drum, a displacer body is inserted into the drum. This causes the water/steam to flow through an annular gap of 8 mm next to the outer shell of the drum.

The material of the outer shell of the drum is austenitic stainless steel (1.4404, similar to ASTM 316 L). In principle, carbon steel is also stable in contact with nitrate salts up to a temperature of at least 390 °C [18,19]. However, as the influence of the scraping process on the corrosion behaviour is not known, 1.4404 stainless steel is used to demonstrate the technology, as it exhibits even better corrosion behaviour in contact with nitrate salts [19]. Since the thermal conductivity of austenitic stainless steel is approximately 18 W/mK, which is significantly lower than that of carbon steel (around 45 W/mK), the use of 1.4404 is not optimal with respect to maximizing heat transfer performance. The influence of the wall thickness of the rotating drum and thus indirectly the influence of the material's thermal conductivity, is discussed in [30], where a decrease in heat transfer of 31% is reported for a specific case when the steel thickness is doubled.

The thickness of the outer pressure-resistant shell of the drum is 7.5 mm. Assuming a yield strength of 127 N/mm^2 at 250 °C [31] and neglecting possible corrosions and weld surcharge, the drum would withstand an internal pressure of up to 54.8 bar. The shell thickness is therefore selected in regards of a safe operation and not optimized for effective heat transfer.

Fig. 5 shows a drawing with the main geometric dimensions of the Rotating Drum Heat Exchanger.

Phase change material

For the storage of thermal energy at high temperatures, nitrate salts and mixtures of nitrate salts have proven to be suitable storage materials for molten salt and latent heat thermal energy storages [12,32]. For the demonstrator, the eutectic mixture of sodium nitrate ($NaNO_3$) and potassium nitrate (KNO_3) ($NaNO_3$/KNO_3(eu)) is used as storage material, as proposed in [20]. The eutectic mixture consists of 50 mol% $NaNO_3$ and 50 mol% KNO_3, which correspond to 45.67 wt% $NaNO_3$ and 54.33 wt% KNO_3 [33]. The melting temperature of 222 °C matches well with the evaporation temperature of water at 8 bar abs of 170 °C, resulting in a temperature difference of at least 52 °C during evaporation. The thermophysical properties of $NaNO_3$/KNO_3(eu) are summarised in

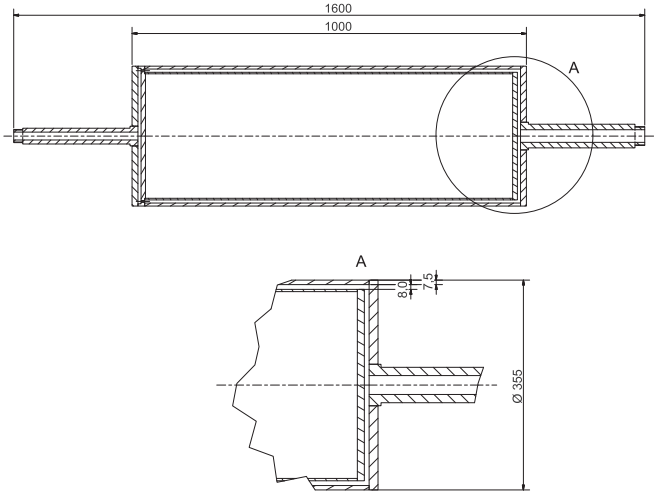

Fig. 5. Drawing of the used Rotating Drum Heat Exchanger and essential geometric properties.

Table 1
Thermophysical properties of the eutectic mixture of sodium nitrate and potassium [20].

Description	Variable	Value	Unit	Remark	Source
Melting point	$T_{PCM,m}$	222	°C		[15]
Phase change enthalpy	L_{PCM}	108	kJ•kg^{-1}		[15]
Thermal conductivity, liquid	$k_{PCM,l}$	0.4574	W•m^{-1}•K^{-1}	222–400 °C	[15]
Thermal conductivity, solid	$k_{PCM,s}$	0.3835	W•m^{-1}•K^{-1}	at 100 °C	[15]
Density, liquid	$\varrho_{PCM,l}$	1965	kg•m^{-3}	at 222 °C	[34]
Density, solid	$\varrho_{PCM,s}$	2055	kg•m^{-3}	at 222 °C	[34]
Viscosity	$\eta_{PCM,l}$	0.00472	Pa·s	at 247 °C	[35]
Heat capacity, liquid	$c_{p,PCM,l}$	1.492	kJ•kg^{-1}•K^{-1}	222 – 350 °C	[15]
Heat capacity, solid	$c_{p,PCM,s}$	1.355	kJ•kg^{-1}•K^{-1}	at 202 °C	[36]
Surface tension	$\sigma_{PCM,l}$	0.1222	N•m^{-1}	at 237 °C	[35]

Table 1 in the storage system described in this paper, 528.6 kg of $NaNO_3/KNO_3$(eu) has been given. After a complete discharge of the system, 393.4 kg of the material has been able to be removed from the cold tank, which means that this amount of PCM has been used during the process. The missing 135.2 kg correspond to PCM residues remaining in dead zones of the system, particularly in the tub below the rotating drum. The current design of the partially immersed rotating drum requires a certain minimum fraction of PCM to remain in the tub beneath the drum to ensure proper operation. However, this fraction can be reduced in future design iterations. Furthermore, by increasing the overall storage capacity and thus the absolute amount of PCM in the hot and cold storage tanks, the relative proportion of unused PCM would decrease.

Design of the scraper

A CW612N brass sheet is used as the blade in contact to the drum surface. Brass is used because of its lower hardness compared to the drums shell made out of 1.4404 stainless steel in order to prevent damage to the surface of the drum. The 1 mm thick brass sheet is fastened between two stainless steel support sheets, also 1 mm thick, with a total of 83 screws on a flat steel bracket. The scraper is moved against the drum by using linear guiding and pressed slightly against the drum with an angel of 32.5°. Fig. 6 shows a drawing of the scraper.

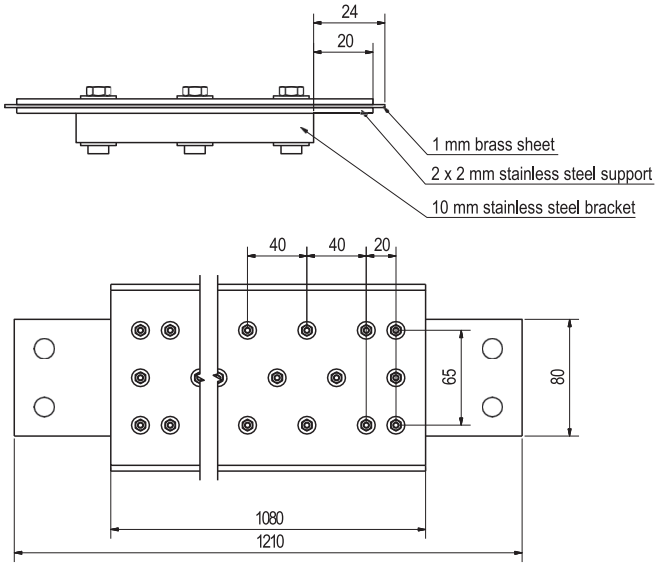

Fig. 6. Drawing of the scraper blade and the support of the scraper.

Experimental methods

Several experiments are performed to demonstrate the storage system. For their analysis, the measuring devices and their accuracy are described in detail, followed by the calculation method. For reproducibility, the performance of the experiments is described using a reference experiment.

Measuring devices and calculation method

The energy transfer at the Rotating Drum Heat Exchanger can be measured using two different methods. In the so-called enthalpy difference method (index Δh), the heat transfer is calculated using the enthalpy of the water at the inlet, the enthalpy of the steam at the outlet as well as the mass flow of water and steam. The so-called temperature difference method (index ΔT) calculates the heat transfer based on the temperature increase in the water reservoir CM301.

For safe operation, the mass flow rate of the water given into the drum has to be around 10% higher than the mass flow rate of steam measured at the outlet of the drum (Compare section 4.2). A two-phase flow must therefore be assumed at the outlet of the drum. The mass flow of water into the drum is measured as by a Coriolis mass flow meter BF101 ($\dot{m}_{101,water}$). The mass flow of steam at the drum's outlet is measured by a vortex measurement device BF102 ($\dot{m}_{102,\,sat.steam}$). Since a vortex flow meter determines the flow velocity of the steam by measuring the frequency of an alternately arranged vortex belt generated behind a bluff body, only the steam phase of the saturated steam flow is measured. On the other hand, there is a minimum Reynold number of the flow required. Therefore, mass flows below around 20 kg/h cannot be detected with the vortex flow meter.

Since the vortex flow meter only determines the mass flow of the steam phase of the two-phase flow, an additional mass flow of saturated water ($\dot{m}_{102,\,sat.water}$) can be calculated by the difference of the mass flow of water measured at the inlet of the drum ($\dot{m}_{101,water}$) and the mass flow of steam measured at the outlet ($\dot{m}_{102,sat.steam}$) by

$$\dot{m}_{102,\,sat.water} = \dot{m}_{101,water} - \dot{m}_{102,sat.steam} \tag{1}$$

The thermal energy transferred at the Rotating Drum Heat Exchanger $\dot{Q}_{RD,\Delta h}$ can be calculated using Eq. (2) via the enthalpy difference multiplied by the respective mass flow:

$$\dot{Q}_{RD,\Delta h} = \left(\dot{m}_{102,\,sat.steam} \bullet h''(T_{sat}, p_{103}) + \dot{m}_{102,sat.\,water} \bullet h'(T_{sat}, p_{103})\right) - \dot{m}_{101,water} \bullet h(T_{106}, p_{102}) \tag{2}$$

Thereby, h' refers to the specific enthalpy of liquid water at the calculated saturation temperature T_{sat}, determined from the measured outlet pressure p_{103}, while h" refers to the specific enthalpy of saturated steam at the same saturation temperature T_{sat}. For the calculation of the enthalpy, REFPROP, mainly based on the IAPWS 1997 formulation, is used. The temperature and the pressure of the water and steam at the drums inlet and outlet is measured by PT100 and pressure transmitter. The assumption of a two-phase flow at the drums outlet with is separated in saturated water and saturated steam is discussed in section 4.2 with experimental data.

Independently of the previous described enthalpy method, the thermal energy transferred at the rotating drum can be estimated via the temperature increase of the water reservoir CM301. Thereby, the thermal energy transferred to the water reservoir CM301 can be calculated by

$$\dot{Q}_{CM301} = \frac{d\overline{T}_{303/304}}{dt} \bullet m_{water,CM301} \bullet c_p\left(\overline{T}_{303/304}\right), \tag{3}$$

with the time-dependent increase d/dt in average temperature $\bar{T}_{303/304}$ of the measured temperatures T_{303} and T_{304} multiplied by the mass of water $m_{water,CM301}$ within the reservoir CM301 and the specific heat capacity of water c_p at the actual temperature. A moving average of 180 s is used to smooth the data for evaluation and visualization in section 4. Neglecting the heat losses and a slight temperature rise in the feed water tank EB101, it applies for the thermal energy transferred at the rotating drum

$$\dot{Q}_{RD,\Delta T} = \dot{Q}_{CM301} - P_{GP301} \tag{4}$$

Thereby, P_{GP301} is the dissipation energy of the Pump GP301 which can be estimated by the nominal electrical power of the pump's engine. It applies $P_{GP301} = 1.1$kW. The mass of water within CM301 has been determined to be 778 kg for the experiments #1 – #3 and 798 kg for experiment #4 according to Table 3. For the used values of the heat capacity c_p of water again REFPROP, based on the IAPWS 1995, is used.

The energy transferred at the rotating drum E_{RD} during the experiment is calculated by an integration of the heat transfer between the start of the experiment t_{Start} and the end of the experiment t_{End} according to

$$E_{RD,\Delta h} = \int_{t_{Start}}^{t_{End}} \dot{Q}_{RD,\Delta h} \bullet dt \tag{5}$$

Since the experimental data are logged every second, the transferred energy in kWh is calculated by

$$E_{RD,\Delta h} = \frac{\sum_{i=0}^{j=i} \dot{Q}_{RD,\Delta h}}{3600}. \tag{6}$$

For a safe operation of the test rig, the level of liquid PCM in the tub below the Rotating Drum Heat Exchanger is measured by a radar level sensor BL201.

The theoretical storage capacity of the storage material between the temperature of the solid, cold storage material T_{cold} and the temperature of the liquid, hot storage material T_{hot} is calculated by

$$E_{PCM} = \left[c_{p,PCM,s} \bullet \left(T_{PCM,m} - T_{cold}\right) + L_{PCM} + c_{p,PCM,l} \bullet \left(T_{hot} - T_{PCM,m}\right)\right] \bullet m_{PCM} \tag{7}$$

with the phase change enthalpy L_{PCM}, the specific heat capacities of the solid phase $c_{p,PCM,s}$ and the specific heat capacities of the liquid phase $c_{p,PCM,l}$ and the melting temperature of the PCM $T_{PCM,m}$ according to Table 1. The measured active mass of PCM in the storage system is $m_{PCM} = 393.4$ kg. Temperature dependent heat capacities of the storage material are neglected within this paper.

In Table 2, the used measuring devices of the test rig and their measuring accuracy are shown. Additionally, the accuracy of the used Siemens analog-to-digital converter are also shown in this table.

For the calculation of the uncertainty of the calculated values, independent variables are assumed. The uncertainty $u_{\dot{Q}}$ of the heat flux $\dot{Q}$ is therefore calculated according to [37] by

$$u_{\dot{Q}} = \sqrt{\sum_{i=1}^{n} \left(\frac{\partial \dot{Q}}{\partial a_i} \Delta a_i\right)^2} \tag{8}$$

with the independent uncertainties Δa_i of the measured values a_i. The combination of the uncertainties of the sensors $\Delta a_{i,sensor}$ and the analog-to-digital conversion $\Delta a_{i,a\text{-}d}$ is assumed to be a simple addition

$$\Delta a_i = \Delta a_{i,sensor} + \Delta a_{i,a-d}. \tag{9}$$

The partial derivation of the enthalpy is calculated by REFPROP. For the partial derivation of enthalpy at the saturation temperature, the temperature is assumed to be 1 K above or below the saturation temperature. Applying Eq. (8) to Eq. (2) for the results given in this paper results in a maximum deviation of ±5.0%, which is a maximum of ±3.4 kW in absolute numbers.

Table 2
Overview of the measurement devices used for evaluation and their accuracy.

Parameter	Sensor Tag	Sensor	Accuracy Sensor $\Delta a_{i,sensor}$	Accuracy Analog-to-digital converter
T_{106}, T_{107}	BT106, BT107	Sheath resistance thermometer PT100, DIN EN 60751, 1/10 DIN/0 °C, 4-wire	1/10 DIN/0 °C ± (0.1 + 0.0017 ·| t |) °C	±1 K
T_{303}, T_{304}	BT303, BT304	Typ K, Class 1 acc. IEC 584–3	±1.5 °C	±2 K
p_{102}, p_{103}	BP102, BP103	piezoresistive absolute pressure sensor, 0…10 bar	0.35% Full Scale Output = 8±0.035 bar	±0.3%
$\dot{m}_{102}$	BF102	Vortex flow meter	±5.7% of reading	±0.3%
$\dot{m}_{101}$	BF101	Coriolis mass flow meter	±0.10% ± [(0.2 ÷ measured value)·100] % of reading	±0.3%
L_{201}	BL201	Radar level sensor	±2 mm	±0.3%
P_{202}	EB202	thyristor regulator with power feedback	±2%	±0.3%

Table 3
Experiments evaluated within this paper.

# No	Date	Description
#1	2024-08-21	Constant discharge cycle, stopped due to empty hot storage tank. Stream pressure: 3 bar (abs), Rotational Speed: 20 rpm
#2	2024-08-28	Continuous decrease of feed water flow, stopped due to incomplete solidification at low inlet mass flow, Stream pressure: 4 bar (abs), Rotational Speed: 20 rpm
#3	2024-08-07	Continuous increase of feed water flow, stopped due to incomplete scrapping at increased rotational speed, Stream pressure: 3 bar (abs), Rotational Speed: 15, 17.5 and 20 rpm. Including repetition of the 20 rpm point from experiment #1
#4	2024-12-03	Constant discharge cycle, stopped due to empty hot storage tank 8 bar (abs), Rotational Speed: 8/12/16/20 rpm

Although thermal insulation is applied to the test rig, heat losses must be considered when interpreting the experimental data. These losses are not explicitly quantified in the above-mentioned equation; however, their possible impact is discussed in Section 4.1.

Description of the experiments

At the start of the experiments, the PCM is in the hot storage tank in the liquid state and tempered to a temperature of 250 °C. Also, the PCM in the tub below the rotating drum is tempered and kept in the liquid state. Since this state usually last for several hours, it is assumed, that there is no liquid water in the drum anymore. Therefore, the experiments start by switching on the pump GP101 with a low mass flow of 10 kg/h. When the temperature T_{107} at the drum's outlet rises towards 100 °C, the rotation of the drum is started at 2.5 rpm in order to homogenize the temperature of the drum shell.

To increase the pressure in the steam system, the automatic steam valve QN102 is set to 1.5 bar (abs), which results in a complete closure of the valve in the beginning. Afterwards, the PCM valve QN201 is opened, liquid PCM flows into the tub below the rotating drum. The drums rotational speed is increased to values of about 10 rpm. When the drum shell starts to have contact with the liquid PCM, the solidification process starts and solid PCM is transported to the scraper, removed from the drum surface and falls into the solid storage tank. When the pressure in the system rises to 1.5 bar, the steam valve QN102 starts to regulate the pressure by opening of the valve. Afterwards, the steam pressure in the

system can be adjusted to a chosen value. The inlet water flow, measured by BF101 is adjusted to be around 10% above the measured flow of steam at the outlet of the drum. The PCM valve QN201 is manually adjusted to keep the level of the liquid PCM in the tub below the PCM constant at around 40% of the capacity of the tub, which results in an immersion depth of the drum of 15°. This corresponds to 4.1% of the total outer drum shell.

The experiment is stopped by closing the PCM valve QN201. The drum is kept rotating until the level of liquid PCM below the drum decreases and the drum shell loses contact to the liquid PCM. In case the scraping process stops, the PCM valve is closed and the rotation of the drum is stopped immediately. Afterwards, the PCM-layer is removed manually from the drum. The rotation is restarted to lower the level of the liquid PCM in the tub below the drum to such an extent that there is no longer any contact with the drum surface.

Fig. 7 shows the bare measured data of the reference experiment. In this paper, four different experiments are used as proof of concept and to discuss the potential of the concept. The three experimental conditions are described in Table 3. The measured data of experiments #2 – #4 are shown in Appendix B.

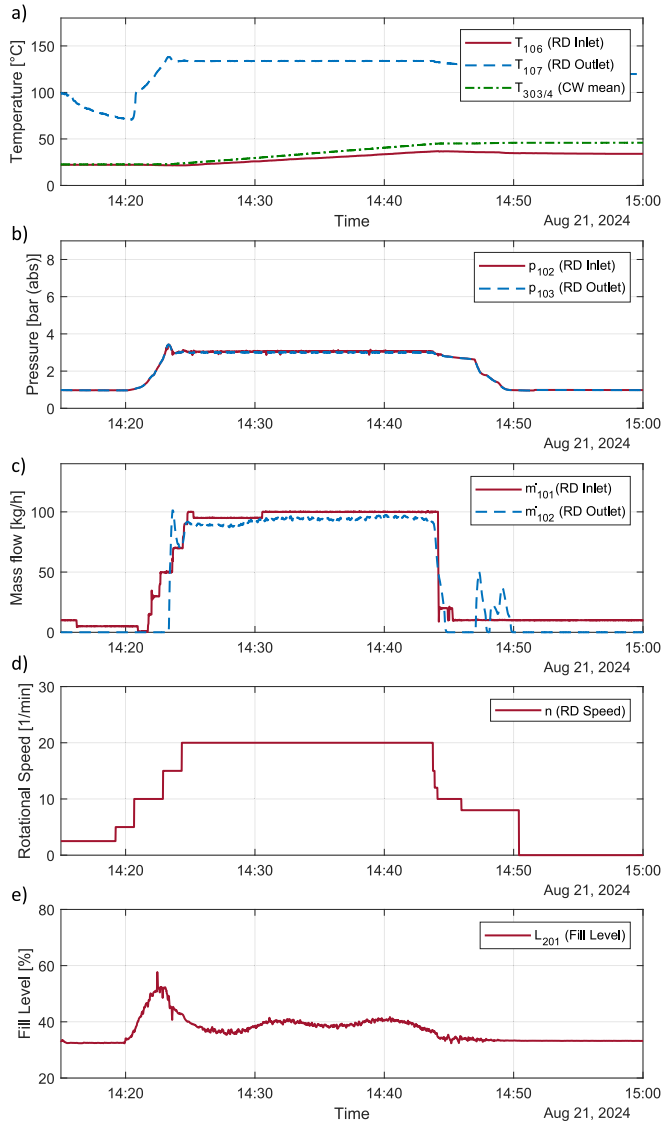

Fig. 7. Data measured during the experiment #1 a) Temperature at the inlet and outlet of the rotating drum as well as in the cooling water Tank b) Pressure at the inlet and the outlet of the rotating drum c) Mass Flow of the water given into the drum and the steam released from the drum d) Rotational Speed of the rotating drum e) Fill level of the tub below the rotating drum.

Experimental results and discussion

In this chapter, the experimental results are analysed and discussed.

Heat transfer at the rotating drum heat exchanger

Fig. 8 shows the heat transfer calculated via the enthalpy difference according to Eq. (1) as well as via the increase in the temperature of the water tank according to Eqs. (2) and (3) for experiment #1. The values of the heat transfer measured using Eq. (1) stabilizes after control-related overshoot at the beginning of the experiment at values of 65 kW. The overshoot results due to the automatic pressure regulation of the steam valve. As the experiment progresses, the heat flow increases and approaches a value of 69 kW. Here, a correlation between the liquid PCM in the tub below the drum, as shown in Fig. 7 e) can be seen. The measured heat transfer decreases to zero when the rotation of the drum is stopped at the end of the experiment. Afterwards, the measured heat transfer peaks twice, which results from the stepwise opening of the steam valve and the release of the pressure within the system.

The heat transfer measured by the temperature increase of the water tank corresponds qualitatively to the values measured via the enthalpy difference. The increase and decrease in heat transfer with time at the beginning and end of the experiment occurs gradually within 180 s, corresponding to the time of the moving average. On average, these values measured by the temperature difference are 12.3% below the values measured via the enthalpy difference. This difference results from the lack of thermal insulation of the piping between the water reservoir CM301 and the condenser EP102, as well as the missing insulation of both, the condenser and the water reservoir itself. The hoses used have an estimated length of approximately 10 m each between the condenser to the water reservoir, while the water reservoir has an uninsulated surface of about 11.25 m^2. Therefore, the discrepancy of both values lies within the expected range and the comparison of the data validates the method of the determination of the heat transfer via the enthalpy method.

The calculated heat transfer for experiment #2, #3 and #4 can be seen in appendix C. Table 4 summarizes the measured average heat transfer at a rotational speed of 20 rpm and the cumulative energy transfer. The cumulative energy transfer is calculated according to Eq. (5) with the values of the heat transfer calculated by the enthalpy

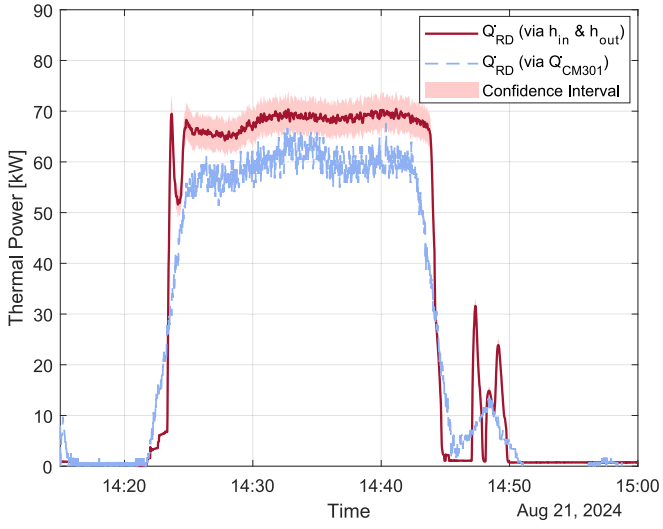

Fig. 8. Heat transfer at the Rotating Drum Heat Exchanger for both calculations, via the enthalpy difference h_{in} and h_{out} and the temperature increase in the water tank CM301 for experiment #1.

Table 4
Overview of the average heat transfer rate and energy transfer.

# No	Pressure [bar abs]	Time Start [hh:mm:ss]	Time End [hh:mm:ss]	Total Duration [mm:ss]	Duration of steam generation [mm:ss]	Heat transfer rate at 20 rpm (via Δh) [kW]	Cumulative Energy Transfer [kWh]
#1	3	14:20:45	14:49:20	28:35	20:31	69.0	23.4
#2	4	10:12:42	10:49:21	36:39	17:13	63.6	18.5
#3	3	13:34:47	14:04:41	29:54	15:55	69.9	16.5
#4	8	09:07:26	09:45:20	37:54	28:54	47.0	15.2

method between the mentioned start and end time of the experiment. The start time of the experiments is defined as the moment when the pressure in the system increases above 1.05 bar abs, while the moment when the pressure in the system decreases below 1.05 bar abs is set as the end of the experiment. The given duration of steam generation is the duration within the experiment, where a steam production within the drum has been measured.

As mentioned in Table 4, a maximal heat transfer of up to 69.9 kW and an energy transfer of up to 23.4 kWh has been demonstrated with the rotating drum. For the demonstration of repeatability, experiment #1 and #3 include both identical operation points at 20 rpm, 3 bar abs and 100 kg/h water inlet. With a relative deviation of 1.3% and an absolute deviation of 0.9 kW, both points are well in the uncertainty range given in Section 3.1.

Influence of inconsistent inlet and outlet mass flow

The Rotating Drum Heat Exchanger with an annual gap at the outer shell of the drum is designed for a consistent inlet and outlet mass flow of water respectively steam. Thereby, the inlet mass flow is controlled to match the outlet flow. Nevertheless, there will always be a mismatch in the inlet and the outlet mass flow, and the effects of this on the behaviour of the Rotating Drum Heat Exchanger is investigated within the following section

In experiment #3, the inlet water flow is increased in three steps to a value 20% above the measured outlet flow. Thereby, no effect on the outlet steam flow, temperature or pressure has been measured. Most likely, the additional water flow leaves the drum together with the steam, which reduces the quality of the steam, but not the thermal power of the drum itself. The vortex flow meter does not detect any change in the volumetric flow. Within Fig. 9, one can see an increase in the mass flow at the drums outlet after 13:50. This increase results from the increase in the rotational speed as can be seen in Appendix B3.

On the other hand, the inlet water flow is reduced in experiment #2 sequentially to a value 16.7% below the measured steam flow. The outlet steam flow remains constant for 3 min and 48 s, but suddenly decreases to a value 2.7% below the inlet mass flow. At this point, it can be assumed that only the amount of water leaves the drum, which is simultaneously given into it, meaning no reservoir of water is left at the lower side of the drum. During the experiment, one could see at the outer side of the drum, that liquid PCM reached the scraper and no solidification occurred. These phenomena started at the steam outlet side of the drum. Therefore, it has to be assumed, that the heat transfer coefficient of the steam is not sufficient to solidify PCM at the outer side of the drum. This behaviour is supported by the measurement of the temperature at the outlet of the drum. Here, no temperature increase can be detected. The experiment has been stopped shortly after liquid PCM reached the scraper due to safety reasons.

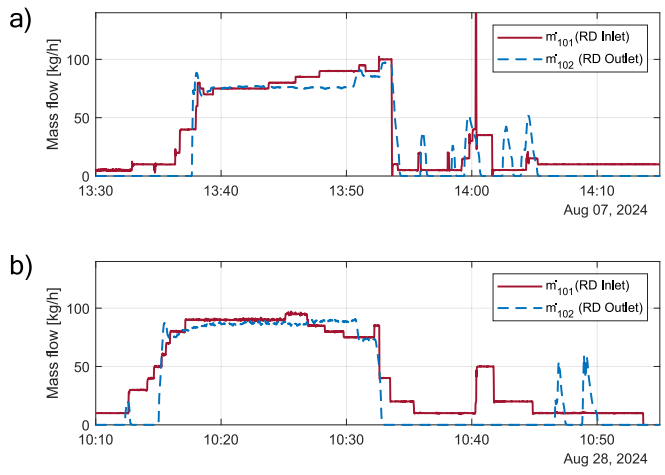

Fig. 9. Variation of the inlet water flow a) for experiment #3 and b) for experiment #2.

As a result of this investigation, the water mass flow into the rotating drum should be maintained at approximately 10% above the steam mass flow measured at the Drum's outlet to ensure stable operation. Under nominal operating conditions, a two-phase flow therefore leaves the drum. To obtain saturated steam suitable for industrial applications, a downstream liquid–vapor separator is required. Such components are well established and readily available for industrial use.

Storage density and utilization of the storage material

Approximately 393.4 kg of NaNO3/KNO3(eu) has been used during one full discharge cycle of the storage system. According to Eq. (9), a measured temperature of the liquid PCM just before the experiments of 250 °C and a measured temperature of the solid PCM of around 170 °C, results in a theoretical storage capacity of 24.07 kWh. During experiment #1, 23.4 kWh of energy has been transferred. Therefore, the utilization rate of the PCM can be calculated to be >95%.

The density of the liquid material at 250 °C can be assumed to be 1940 kg/m^3, the one of the solid phase at 170 °C to be 2193 kg/m^3 [15]. With the measured transferred heat of 23.4 kWh and a mass of the storage material of 393.4 kg, the demonstrated volumetric storage density of the liquid phase of 115 kWh/m^3 is obtained. Regarding the solid phase, the porosity of the solid particles has to be considered in the calculation. With a simple measurement of the porosity by measuring the weight of a vessel with a volume of 30 l filled with the particles, a porosity of 65% is calculated. Therefore, the volumetric storage density of the solid phase is decreased to a value of 45 kWh/m^3. Nevertheless, for industrial application, cost benefits for the cold storage tank can be assumed, since the material is not liquid and comparable cold. Furthermore, the demonstrated storage density within this paper can be increased by increasing the temperatures of the liquid storage material as mentioned in section 1. Furthermore, the use of pure $NaNO_3$ with a melting point of 306 °C would increase the specific energy storage density as well as the surface specific heat transfer due to a higher temperature difference between the melting point of the PCM and the saturation temperature of the evaporating water as reported in [20].

The scope of this work is limited to a prove of the discharge cycle, specifically the generation of steam through the utilization of latent heat from the phase change and, to a lesser extent, the sensible heat of the liquid and solid PCM. The PCM-side is not independently quantified, including thermal losses within the liquid and solid phase. Furthermore, the electrical energy for charging the system has not been measured.

Therefore, an overall full cycle efficiency is not reported in this study. For industrial-scale applications, i.e., storage capacities in the GWh range, the overall system losses will be dominated by thermal losses from the storage tanks. In this context, reference can be made to operational experience with large-scale molten salt storage systems, which demonstrate storage efficiencies in the range of approximately 99% [38].

Surface specific heat transfer density

The total outer shell surface of the drum used is 1.115 m^2. During the experiments, the level of the liquid PCM is regulated to 40% of the fill level of the tub below the rotating drum. This results in a submersion angle of the drums shell of 15°. This corresponds to 4.1% of the total drum shell or 0.046 m^2 in absolute surface. Due to the adhering liquid PCM at the drums outer surface, solidification occurs also when the surface has already left the tub of liquid PCM. Therefore, the maximum measured heat transfer of 69.9 kW is referred to the total drum shell, which results in a heat transfer density of 60.4 kW/m^2. Referring the maximum measured heat transfer to the immersed shell surface only, a heat transfer density of 1520 kW/m^2 would result. The affecting temperature difference in the process can be assumed to be the difference between the evaporation temperature of the water within the drum and the solidification temperature of the PCM of 222 °C. Thereby, the evaporation temperature of the water within the drum can be changed by the pressure. In the experiments, the pressure has been variated to be 3 bar (abs), 4 bar (abs) and 8 bar (abs), resulting in an evaporation temperature of 133.5 °C, 143.6 °C and 170.4 °C. This results in a temperature difference as mentioned of 88.5 K, 78.4 K and 51.6 k.

In Fig. 10, the measured total heat transfer as well as the surface specific heat transfer is shown as a function of the temperature difference. The total heat transfer increases proportionally with the temperature difference, consistent with the driving force for heat conduction – as is also the case in conventional heat exchangers. The increase of the total heat transfer can be quantified to be 600 W per K. On the other hand, the surface specific heat transfer is also varying for different temperature differences, which is not the case in conventional heat exchangers. Thereby, the surface specific heat transfer decreases with higher temperature differences and can be quantified to be −3.1 W/m^2K per each increased K on average.

The maximum absolute value measured for the surface specific heat transfer is 0.817 kW/m^2K at a temperature difference of 51.6 K. A heat transfer coefficient between the actual drum wall temperature and the liquid PCM temperature was not determined in this study, since the wall temperature was not specifically measured. The scope of this work is in the demonstration of a Rotating Drum Heat Exchanger and the value can be maximized by further work.

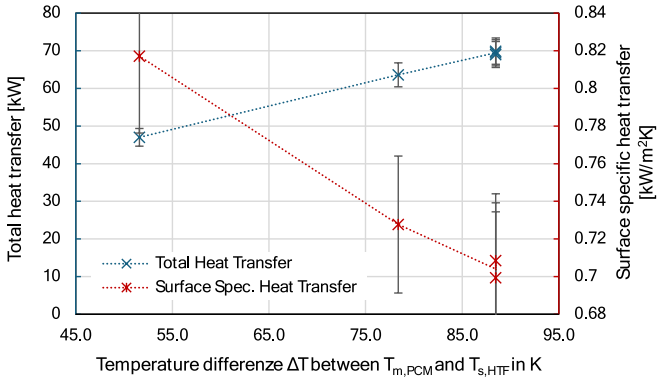

Fig. 10. Measured total heat transfer and surface specific heat transfer for different temperature differences.

Qualitative evaluation and discussion of the scraping process

In this study, several tests have been conducted to find an improved method to remove the PCM from the rotating drum, which resulted in the scraper design as shown in Section 2.5.. In the experiments presented, the PCM is completely removed from the drum surface, leaving no residual layer and allowing a bare surface to re-enter the PCM. However, with increasing operating time of the scraper blade (typically around 1 h) or at rotational speeds above 20 rpm, which result in very thin layer thicknesses, small amounts of PCM remain on the drum surface. Shortly thereafter (e.g., after approximately 20 s), the scraper blade is forced away from the drum surface due to the accumulation of unremoved PCM. Consequently, the experiments had to be stopped and the remaining PCM was removed manually. Since the scraper material was intentionally selected to be softer than the material of the rotating drum, wear was observed exclusively on the scraper blade, while no surface degradation was detected on the rotating drum. In summary, the scraping process is inherently sensitive but remains controllable within certain operating limits. Nevertheless, further evaluation of the scraping process is required, including potential surface treatment of the drum and the investigation of alternative scraping methods.

The nominal electrical power of the engine used to rotate the drum is 2.2 kW. Since a frequency inverter has been used to control the rotational speed of the drum, a measurement of the electrical consumption of the engine is only possible with increased financial effort and has not been conducted within the experiment. Nevertheless, dividing the nominal electrical consumption of 2.2 kW by the minimal measured thermal power of 47 kW results in parasitic energy consumption of 4.6%. Since there is no evidence that the engine has ever run on full load, a parasitic energy consumption of below 0.5% can be assumed for a large-scale steam generator. In Fig. 11, flakes of the PCM after being scraped off the rotating drum are showed.

Conclusion and outlook

In this work, an active LHTES system based on the Rotating Drum Heat Exchanger has been successfully demonstrated in multi-kW and multi-kWh range. For the first time, steam generation has been provided using an active concept, marking a significant milestone in the development of active LHTES. Thereby, the system has been demonstrated supplying saturated steam with a pressure of up to 8 bar abs.

For the determination of the heat transfer, two independent methodologies are described: A method based on the enthalpy difference of the water/steam at the inlet and outlet of the drum and a method using the temperature increase of a water reservoir use for the condensation of the produced steam. The calculated heat transfer of the enthalpy method thereby increases the values calculated with the temperature difference

Fig. 11. PCM flakes after being scraped off the rotating drum.

method by 12.3% on average. This can be explained by heat losses in the piping and the water reservoir. This establishes a solid foundation for the characterization of the system with the enthalpy method. Within the described experiments, steam supply with a pressure of 3 bar (abs), 4 bar (abs) and 8 bar (abs) has been demonstrated. The maximum measured heat transfer has been estimated to be 69.9 kW, which results in a surface specific heat transfer of 60.4 kW/m^2 when referred to the total drums surface. Based on this, operational parameters as the rotational speed of the drum, the immersion angle into the liquid PCM, the pressure and saturation temperature of the water inside the drum, and the temperature of the water at the inlet into the drum can now be systematically varied and analysed for a full characterisation of the technology. Within the experimental test rig, 393.4 kg of the eutectic mixture of KNO_3 and $NaNO_3$ has been used as storage material, having a melting point of 222 °C. Thereby, up to 23.4 kWh has been stored with the material heated up to 250 °C.

Looking forward, long-duration testing will be critical, particularly to assess the mechanical durability and performance stability of the scraper. From a heat transfer perspective, the surface-specific heat transfer is already comparable to those of conventional fossil-fuel-based steam generators. However, there remains significant potential for increasing heat transfer density through design optimizations of the drum geometry. Additionally, replacing the currently used eutectic mixture of $NaNO_3$ and KNO_3 with pure technical grade $NaNO_3$ with a melting point of 306 °C as PCM will further enhance the thermal performance due to higher available temperature difference between the melting point of the PCM and the temperature of the water evaporating inside the drum. Beyond this, the use of other high-temperature PCMs, such as carbonates and chlorides, may also be considered. However, this requires further investigation, particularly with respect to sealing technology and corrosion resistance.

This work lays the foundation for further development of active LHTES toward a commercially viable, high-efficiency thermal energy storage solution, enabling flexible and sustainable steam generation in industrial applications.

CRediT authorship contribution statement

Jonas Tombrink: Writing – original draft, Visualization, Validation, Methodology, Investigation, Funding acquisition, Conceptualization. **Andrea Gutierrez:** Writing – review & editing, Supervision.

Funding

This research did not receive any specific grant from funding agencies in the public, commercial, or not-for-profit sectors.

Declaration of competing interest

The authors declare that they have no known competing financial interests or personal relationships that could have appeared to influence the work reported in this paper.

Appendix A. P&ID of the experimental test rig

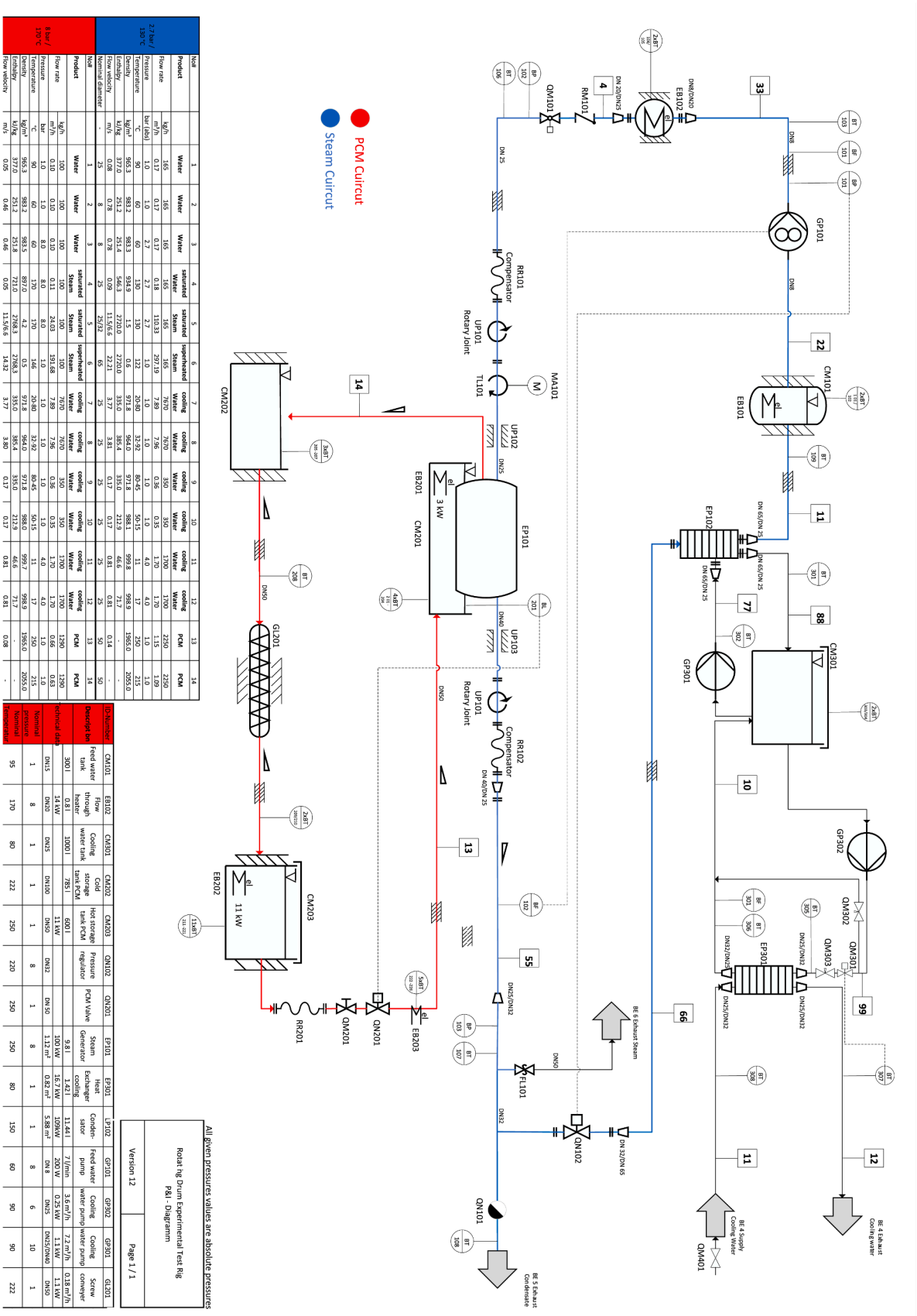

Nod		1	2	3	4	5	6	7	8	9	10	11	12	13	14
Product		Water	Water	Water	saturated Steam	saturated Steam	superheated Steam	cooling Water	cooling Water	cooling Water	cooling Water	cooling Water	cooling Water	PCM	PCM
Flow rate	kg/h	165	165	165	165	165	165	7670	7670	350	350	1700	1700	2250	2350
	m³/h	0.17	0.17	0.17	0.18	110.33	297.19	7.89	7.96	0.36	0.35	1.70	1.70	1.15	1.09
Pressure	bar (abs)	1.0	1.0	1.7	2.7	27	27	1.0	1.0	1.0	1.0	4.0	4.0	1.0	1.0
Temperature	°C	90	90	90	130	130	130	25	25	25	25	25	25	50	50
Density	kg/m³	965.3	983.2	983.3	934.9	1.9	0.6	971.8	964.0	988.1	999.8	988.9	999.8	1965.0	2055.0
Enthalpy	kJ/kg	377.0	251.2	251.4	546.3	2720.0	2720.0	335.0	385.4	212.9	46.6	71.7	46.6	-	-
Flow velocity	m/s	0.08	0.78	0.78	0.09	11.5/6.6	22.71	3.77	3.81	0.17	0.17	0.81	0.81	0.14	-
Nominal diameter	-	25	8	8	25	25/32	65	25	25	25	25	25	25	50	50
Nod		1	2	3	4	5	6	7	8	9	10	11	12	13	14
Product		Water	Water	Water	saturated Steam	saturated Steam	superheated Steam	cooling Water	cooling Water	cooling Water	cooling Water	cooling Water	cooling Water	PCM	PCM
Flow rate	kg/h	100	100	100	100.00	100.00	100.00	7670.0	7670.0	350.0	350.0	1700.0	1700.0	1290	1290
	m³/h	0.10	0.10	0.10	0.11	24.03	59.07	7.89	7.96	0.36	0.35	1.70	1.70	0.66	0.63
Pressure	bar	1.0	1.0	8.0	8.0	8.0	1.0	1.0	1.0	1.0	1.0	4.0	4.0	1.0	1.0
Temperature	°C	90	60	60	170	170	146	20.80	32.92	80.45	50.15	11	17	250	215
Density	kg/m³	965.3	983.2	983.5	897.0	4.2	0.5	971.8	964.0	971.8	988.0	999.7	998.9	1965.0	2095.0
Enthalpy	kJ/kg	377.0	251.2	251.8	721.0	2768.3	2768.3	335.0	385.4	335.0	212.9	46.6	71.7	-	-
Flow velocity	m/s	0.05	0.46	0.46	0.05	11.5/6.6	14.32	3.77	3.80	0.17	0.17	0.81	0.81	0.28	-

Nr./Nummer		CM101	EB102	CM301	CM202	CM203	QN102	QN201	EP101	EP301	LP102	GP101	GP302	GP301	GL201
Descript ion	Feed water tank	Flow through heater	Cooling water tank	Cold storage tank PCM	Hot storage tank PCM	Pressure regulator	PCM Valve	Steam Generator	Heat Exchanger cooling	Conden-sator	Feed water pump	Cooling water pump	Cooling water pump	Screw conveyer
Technical data	300 l	0.8 l 14 kW	1000 l	785 l	600 l			9.8 l 100 kW	1.42 l 16.7 kW	11.44 l 109kW	7 l/min 200 W	3.6 m³/h 0.25 kW	7.2 m³/h 1.1 kW	0.18 m³/h 1.1 kW
Nominal pressure	DN 15	DN 20	DN 25	DN 100	DN 50	DN 32	DN 50	1.12 m²	0.82 m²	5.88 m²	DN 8	DN 25	DN 25/DN 40	DN 50
Nominal temperatu	1	8	1	1	1	8	1	8	1	1	8	6	10	1
	95	170	80	222	250	220	250	250	80	150	60	90	90	222

All given pressures values are absolute pressures

Rotat hg Drum Experimental Test Rig P&I - Diagramm	
Version 12	Page 1 / 1

Fig. A1. P&ID in full detail of the experimental test rig.

Appendix B. Experimental data in full detail

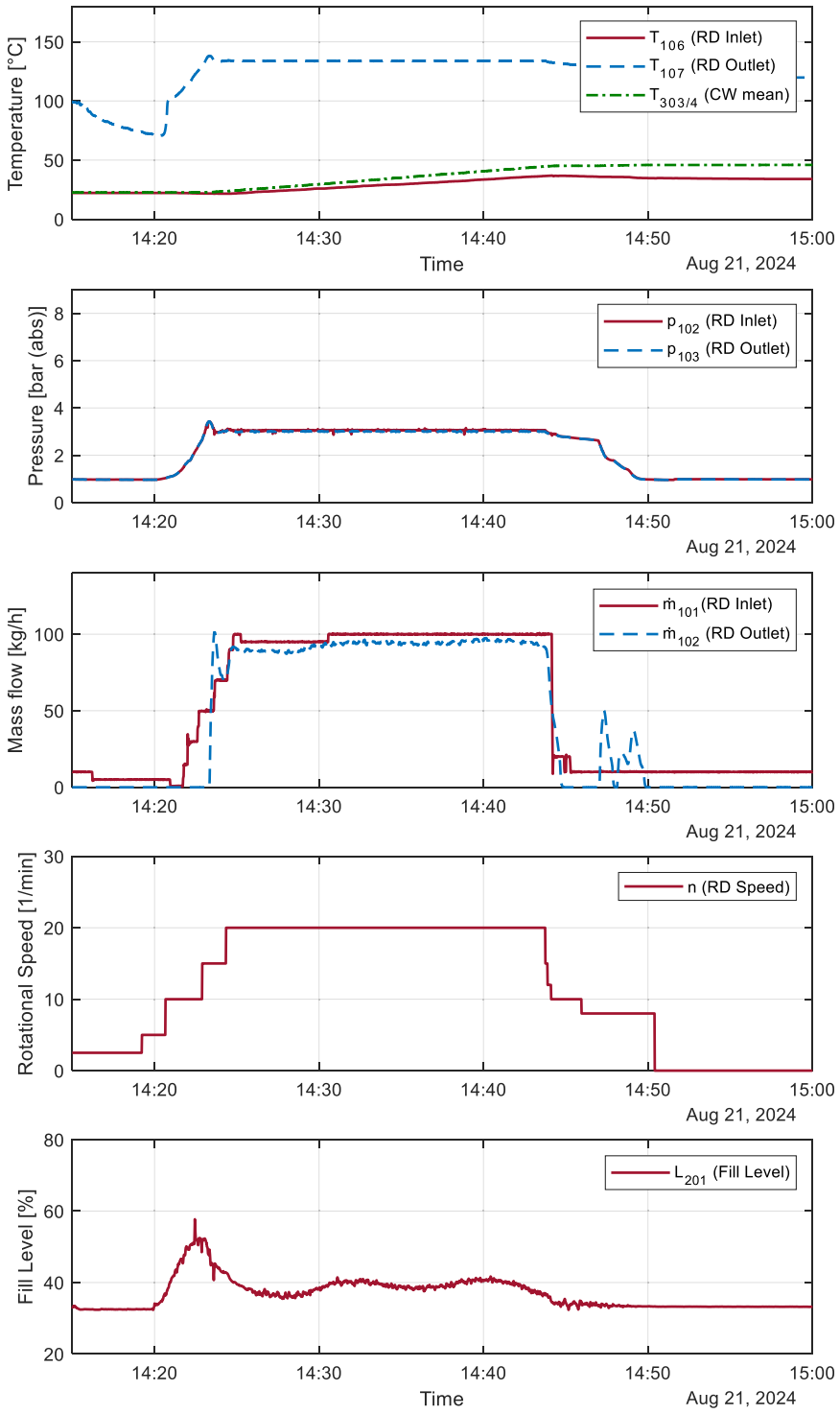

Fig. B1. Data measured during the experiment #1, identical to Fig. 7 a) Temperature at the inlet and outlet of the rotating drum as well as in the cooling water Tank b) Pressure at the inlet and the outlet of the rotating drum c) Mass Flow of the water given into the drum and the steam released from the drum d) Rotational Speed of the rotating drum e) Fill level of the tub below the rotating drum.

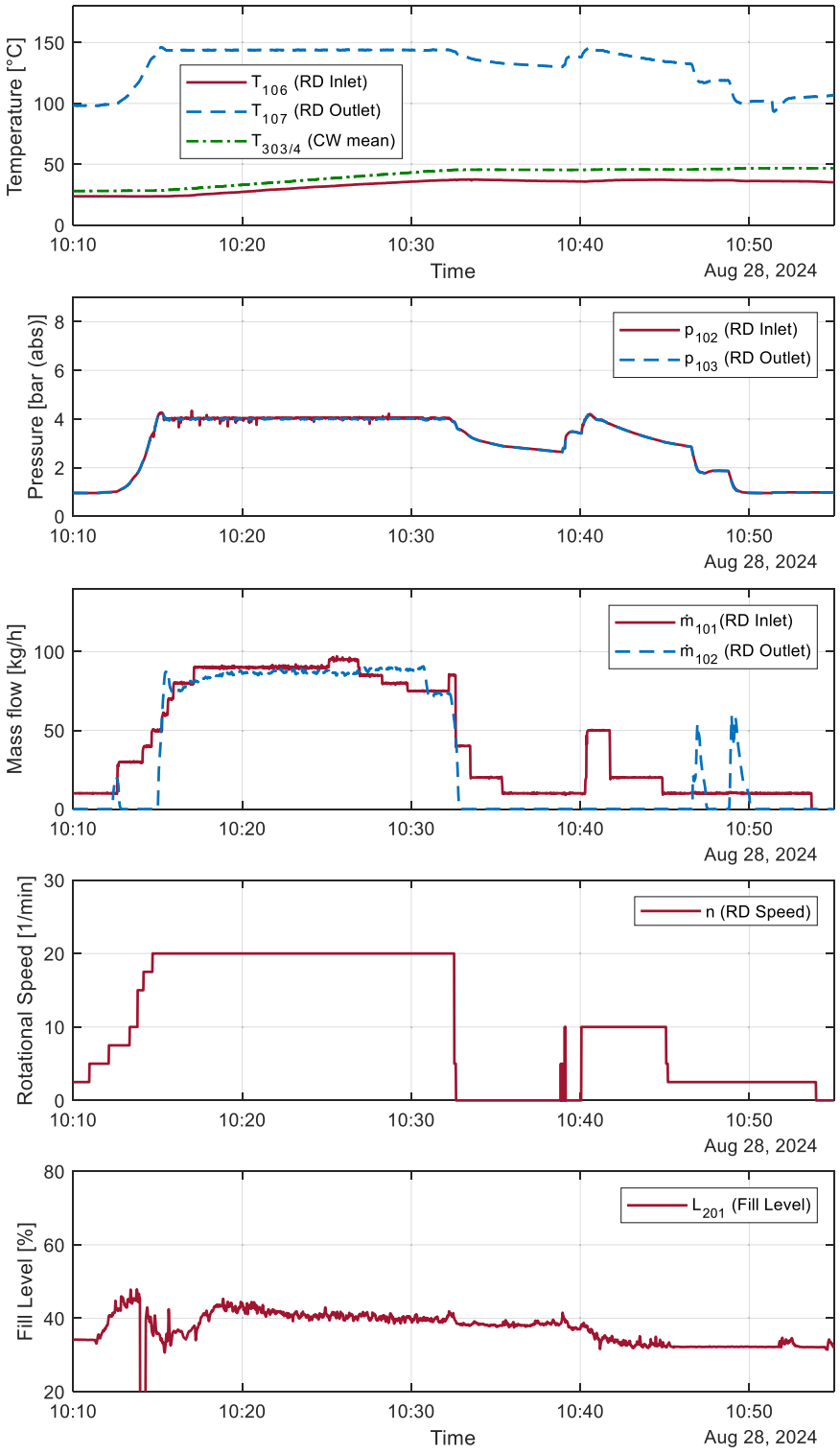

Fig. B2. Data measured during the experiment #2 a) Temperature at the inlet and outlet of the rotating drum as well as in the cooling water Tank b) Pressure at the inlet and the outlet of the rotating drum c) Mass Flow of the water given into the drum and the steam released from the drum d) Rotational Speed of the rotating drum e) Fill level of the tub below the rotating drum.

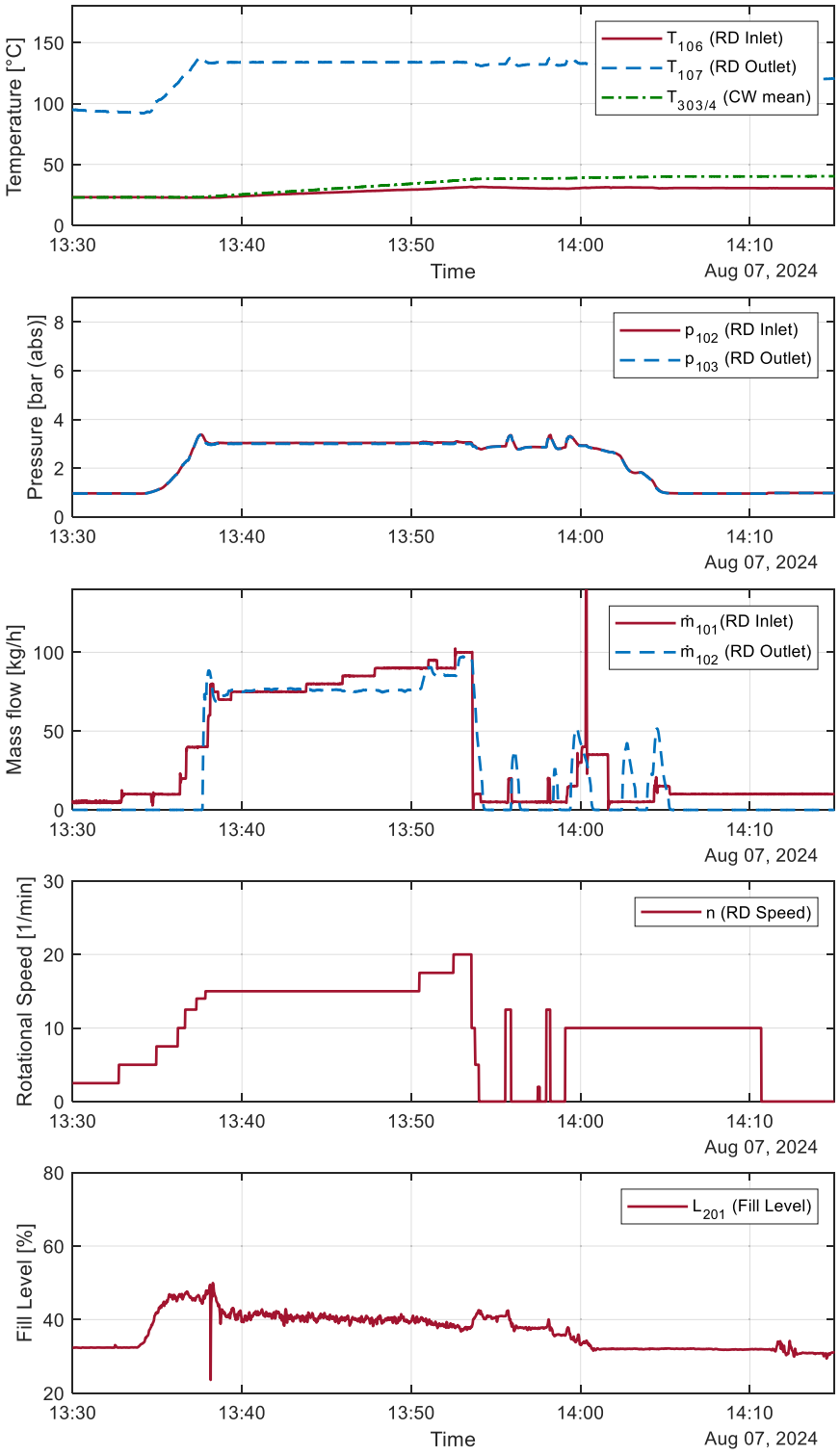

Fig. B3. Data measured during the experiment #3 a) Temperature at the inlet and outlet of the rotating drum as well as in the cooling water Tank b) Pressure at the inlet and the outlet of the rotating drum c) Mass Flow of the water given into the drum and the steam released from the drum d) Rotational Speed of the rotating drum e) Fill level of the tub below the rotating drum.

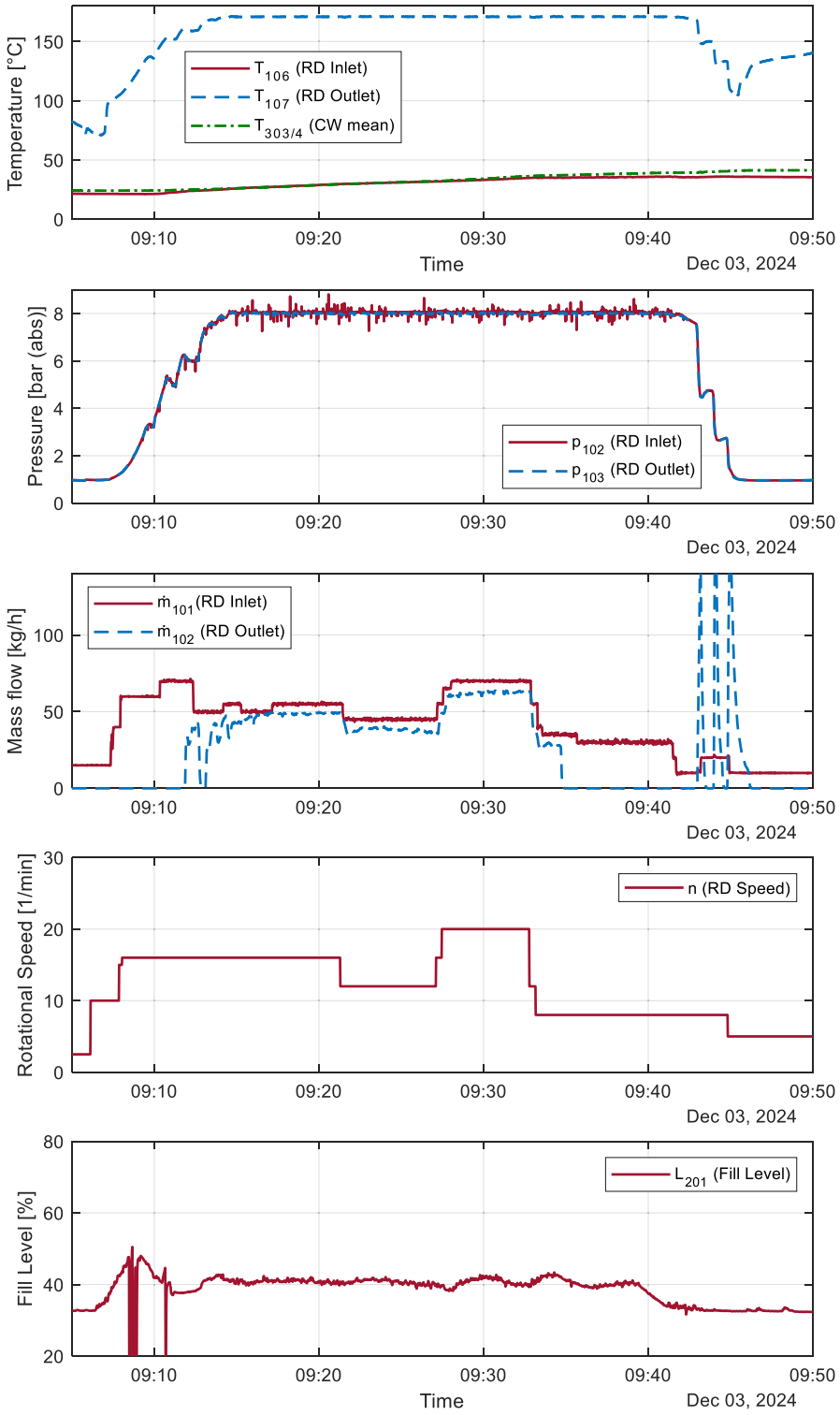

Fig. B4. Data measured during the experiment #4 a) Temperature at the inlet and outlet of the rotating drum as well as in the cooling water Tank b) Pressure at the inlet and the outlet of the rotating drum c) Mass Flow of the water given into the drum and the steam released from the drum d) Rotational Speed of the rotating drum e) Fill level of the tub below the rotating drum.

Appendix C. Calculated heat transfer at the rotating drum of the experiments

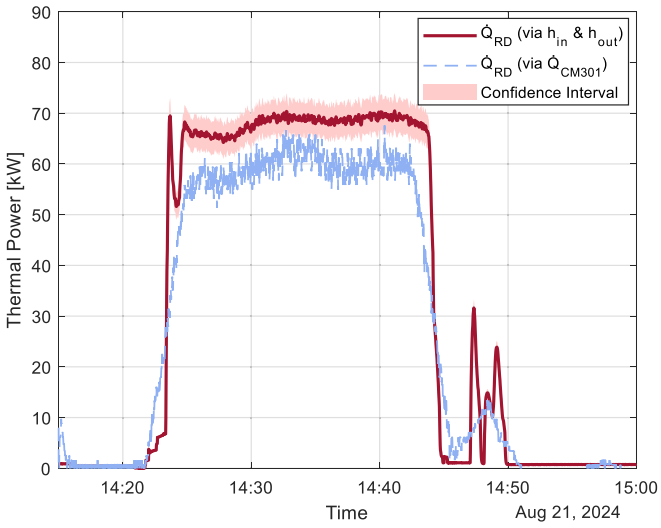

Fig. C1. Calculated heat transfer in kW of experiment #1, calculated via the enthalpy method (via hin and hout) and via the temperature increase in CM301 (via QCM301).

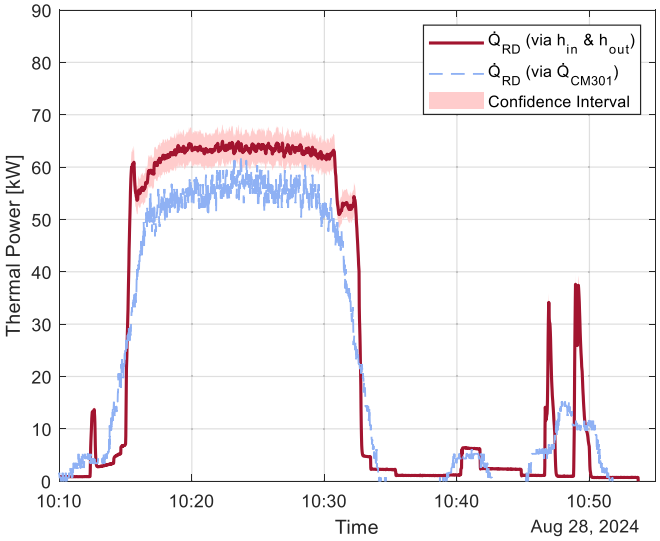

Fig. C2. Calculated heat transfer in kW of experiment #2, calculated via the enthalpy method (via hin and hout) and via the temperature increase in CM301 (via QCM301).

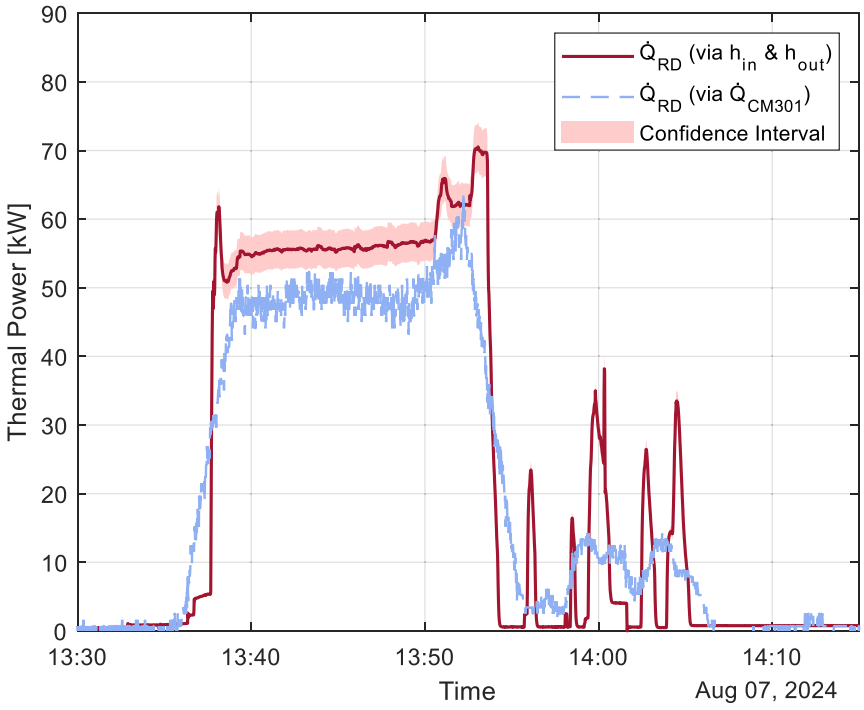

Fig. C3. Calculated heat transfer in kW of experiment #3, calculated via the enthalpy method (via hin and hout) and via the temperature increase in CM301 (via QCM301).

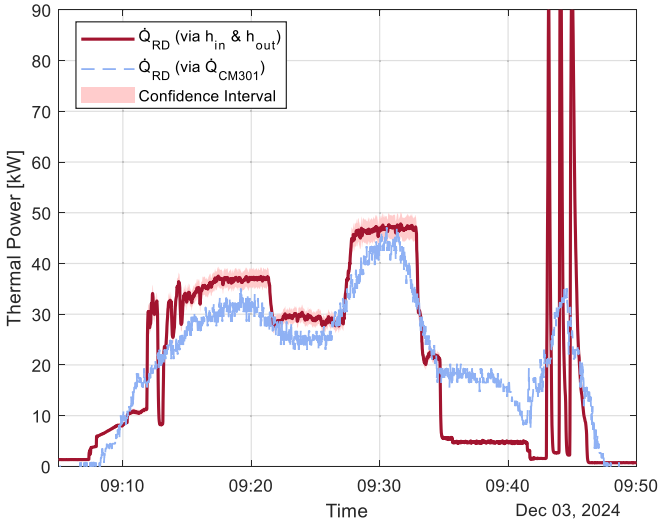

Fig. C4. Calculated heat transfer in kW of experiment #1, calculated via the enthalpy method (via hin and hout) and via the temperature increase in CM301 (via QCM301).

Data availability

Data will be made available on request.

References

[1] Renewables 2023, Analysis and forecast to 2028. International Energy Agency (IEA), 2024.
[2] Naegler T, Simon S, Klein M, Gils HC. Quantification of the European industrial heat demand by branch and temperature level. Int J Energy Res 2015;39:2019–30. https://doi.org/10.1002/er.3436.
[3] Rehfeldt M, Fleiter T, Toro F. A bottom-up estimation of the heating and cooling demand in European industry. Energ Effi 2017;11:1057–81. https://doi.org/10.1007/s12053-017-9571-y.
[4] Ziarkash W, Bünning S, Bensmann A, Baake E, Hanke-Rauschenbach R. A comparative analysis of low-CO2 steam generation technologies. Energy Conv Manag: X 2025;26:101013. https://doi.org/10.1016/j.ecmx.2025.101013.
[5] Renewable Power Generation Costs in 2023. International Renewable Energy Agency (IRENA), Abu Dhabi, 2024.
[6] Mahnoor M, Chandio R, Inam A, Ahad IU. Critical and strategic raw materials for energy storage devices. Batteries 2025;11:163. https://doi.org/10.3390/batteries11040163.
[7] Arpagaus C, Bless F, Uhlmann M, Schiffmann J, Bertsch SS. High temperature heat pumps: Market overview, state of the art, research status, refrigerants, and application potentials. Energy 2018;152:985–1010. https://doi.org/10.1016/j.energy.2018.03.166.
[8] Marina A, Spoelstra S, Zondag H, Wemmers A. An estimation of the European industrial heat pump market potential. Renew Sustain Energy Rev 2021;139:110545. https://doi.org/10.1016/j.rser.2020.110545.
[9] Wang R, Yan H, Wu D, Jiang J, Dong Y. High temperature heat pumps for industrial heating processes using water as refrigerant. Energy 2024;313:133847. https://doi.org/10.1016/j.energy.2024.133847.
[10] Ma X, Du Y, Zhao T, Zhu T, Lei B, Wu Y. A comprehensive review of compression high-temperature heat pump steam system: Status and trend. Int J Refrig 2024;164:218–42. https://doi.org/10.1016/j.ijrefrig.2024.04.024.

[11] Trevisan S, Pathi S, Brown J, Buchbjerg B, Borrero AB, Guedez R. Thermal performance and dynamic response assessment of an industrial molten salts based power-to-heat system. Energy Conv Manag 2025;342:120131. https://doi.org/10.1016/j.enconman.2025.120131.
[12] Bauer T, Odenthal C, Bonk A. Molten salt storage for power generation. Chem Ing Tech 2021;93:534–46. https://doi.org/10.1002/cite.202000137.
[13] G. Glatzmaier. Developing a Cost Model and Methodology to Estimate Capital Costs for Thermal Energy Storage. Golden, CO (United States), 2011. https://doi.org/10.2172/1031953.
[14] Bonk A, Braun M, Sötz V, Bauer T. Solar salt – pushing an old material for energy storage to a new limit. Appl Energy 2020;262:114535. https://doi.org/10.1016/j.apenergy.2020.114535.
[15] Bauer T, Laing D, Tamme R. Overview of PCMs for Concentrated Solar Power in the Temperature Range 200 to 350°C. Adv Sci Technol 2010;74:272–7. https://doi.org/10.4028/www.scientific.net/AST.74.272.
[16] Bauer T, Laing D, Tamme R. Characterization of sodium nitrate as phase change material. Int J Thermophys 2011;33:91–104. https://doi.org/10.1007/s10765-011-1113-9.
[17] Jriri T, Rogez J, Bergman C, Mathieu J. Thermodynamic study of the condensed phases of NaNO3, KNO3 and CsNO3 and their transitions. Thermochim Acta 1995;266:147–61. https://doi.org/10.1016/0040-6031(95)02337-2.
[18] Ruiz-Cabañas FJ, Prieto C, Osuna R, Madina V, Fernández AI, Cabeza LF. Corrosion testing device for in-situ corrosion characterization in operational molten salts storage tanks: A516 Gr70 carbon steel performance under molten salts exposure. Sol Energ Mat Sol Cells 2016;157:383–92. https://doi.org/10.1016/j.solmat.2016.06.005.
[19] Goods SH, Bradshaw RW. Corrosion of stainless steels and carbon steel by molten mixtures of commercial nitrate salts. J Mater Eng Perform 2004;13:78–87. https://doi.org/10.1361/10599490417542.
[20] Tombrink J, Bauer D. Demand-based process steam from renewable energy: Implementation and sizing of a latent heat thermal energy storage system based on the Rotating Drum Heat Exchanger. Appl Energy 2022;321:119325. https://doi.org/10.1016/j.apenergy.2022.119325.
[21] Tombrink J, Jockenhofer H, Bauer D. Experimental investigation of a rotating drum heat exchanger for latent heat storage. Appl Therm Eng 2020;183:116221. https://doi.org/10.1016/j.applthermaleng.2020.116221.
[22] Tombrink J, Bauer D. Simulation of a rotating drum heat exchanger for latent heat storage using a quasistationary analytical approach and a numerical transient finite difference scheme. Appl Therm Eng 2021;194:117029. https://doi.org/10.1016/j.applthermaleng.2021.117029.
[23] Jegadheeswaran S, Sundaramahalingam A, Pohekar DS. Alternative heat transfer enhancement techniques for latent heat thermal energy storage system: a review. Int J Thermophys 2021;42:171. https://doi.org/10.1007/s10765-021-02921-x.
[24] Shank K, Tiari S. A review on active heat transfer enhancement techniques within latent heat thermal energy storage systems. Energies 2023;16:4165. https://doi.org/10.3390/en16104165.
[25] Yang ZL, Walvekar R, Wong WP, Sharma RK, Dharaskar S, Khalid M. Advances in phase change materials, heat transfer enhancement techniques, and their applications in thermal energy storage: a comprehensive review. J Energy Storage 2024;87:111329. https://doi.org/10.1016/j.est.2024.111329.
[26] Huang X, Du Z, Liu Z, Yang X, Sundén B. Research progress of fin design in latent heat energy storage enhancement technology. Appl Therm Engineering 2025;278:127157. https://doi.org/10.1016/j.applthermaleng.2025.127157.
[27] Johnson M, Fiss M. Superheated steam production from a large-scale latent heat storage system within a cogeneration plant. Commun Eng 2023;2:68. https://doi.org/10.1038/s44172-023-00120-0.
[28] Fu W, Yan X, Gurumukhi Y, Garimella VS, King WP, Miljkovic N. High power and energy density dynamic phase change materials using pressure-enhanced close contact melting. Nat Energy 2022;7:270–80. https://doi.org/10.1038/s41560-022-00986-y.
[29] Agegnehu B, Liebezeit K, Fasano M, Morciano M, Chiavazzo E. Dynamic PCM for high-performance latent thermal energy storage: a numerical and parametric study. Int Commun Heat Mass Transf 2025;167:109277. https://doi.org/10.1016/j.icheatmasstransfer.2025.109277.
[30] Mills KC. Recommended values of thermophysical properties for selected commercial alloys. Abington: Woodhead Publishing Limited; 2002.
[31] E.C.f. Standardization, Stainless steels - Part 3. Technical delivery conditions for semi-finished products, bars, rods and sections for general purposes, EN 10088-3, 2014. https://dx.doi.org/10.31030/2102108.
[32] Orozco M, Acurio K, Vásquez-Aza F, Martínez-Gómez J, Chico-Proano A. Thermal storage of nitrate salts as phase change materials (PCMs). Materials (Basel) 2021;23:7223. https://doi.org/10.3390/ma14237223.
[33] Zhang X, Tian J, Xu K, Gao Y. Thermodynamic evaluation of phase equilibria in NaNO3-KNO3 system. J Phase Equilib 2003;24:441–6. https://doi.org/10.1361/105497103770330091.
[34] H. Schinke, F. Sauerwald. Dichtemessungen. Über die Volumenänderung beim Schmelzen und den Schmelzprozeß bei anorganischen Salzen. J Inorg Gen Chem 1960;304:25-36. https://doi.org/10.1002/zaac.19603040104.
[35] Janz GJ, Krebs U, Siegenthaler HF, Tomkins RPT. Molten salts: volume 3 nitrates, nitrites, and mixtures: electrical conductance, density, viscosity, and surface tension data. J Phys Chem Ref Data 1972;1:581–746. https://doi.org/10.1063/1.3253103.
[36] R.W. Carling, C.M. Kramer, R.W. Bradshaw, D. A. Nissen, S. H. Goods, R. W. Mar, J. W. Munford, M. M. Karnowsky, R. N. Biefeld, N. J. Norem. Molten nitrate salt technology development status report SAND80-8052, 1981.
[37] R.J. Taylor. An Introduction to Error Analysis: The Study of Uncertainties in Physical Measurements, 2nd ed. 1997 Edition ed., Sausalito, California: University Science Books, 1997.
[38] Prieto C, Blindu A, Cabeza LF, Valverde J, García G. Molten salts tanks thermal energy storage: aspects to consider during design. Energies 2024;22:17. https://doi.org/10.3390/en17010022.
[39] California Independent System Operator (CAISO) Wholesale Electricity Dashboard, U.S. Energy Information Administration, [Online]. Available: https://www.eia.gov/electricity/wholesalemarkets/caiso.php. [Accessed 20 10 2024]. (between 07/25 and 09/05 values of 2024 has been used since values in 2023 are missing),".
[40] entsoe Transparency Platform, ENTSO-E, 2024. [Online]. Available: https://transparency.entsoe.eu/. [Accessed 24 10 2024].